



ELSEVIER



Available online at www.sciencedirect.com

ScienceDirect

Procedia Engineering 100 (2015) 1714 – 1723

Procedia
Engineering

www.elsevier.com/locate/procedia

25th DAAAM International Symposium on Intelligent Manufacturing and Automation, DAAAM 2014

Analysis and Simulation of New Wheel Pair Construction

Alexander Shiler*

Omsk State Transport University, Pr. Marksa 35, 644046 Omsk, Russia

Abstract

For development of railway transport it is important to have reliable, power effective cars. Cars reliability and efficiency strongly depend on a wheel pair construction. To satisfy these needs a wheel pair for a new cars generation was designed. New design has following features: flexible bandage with cylindrical a surface, the wheel center established on own bearings, independent wheel treads. Article investigates design and modeling of new wheel pair movement. Research of wheel pair was conducted using simulation of wheel flange loaded conditions. The optimal flange form is found and analyzed.

© 2015 Published by Elsevier Ltd. This is an open access article under the CC BY-NC-ND license

(<http://creativecommons.org/licenses/by-nc-nd/4.0/>).

Peer-review under responsibility of DAAAM International Vienna

Keywords: new wheel pair; power effective cars; increase axial loading; reduce wear; analysis and simulation

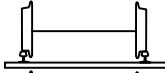
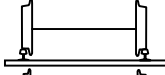
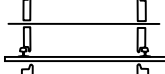
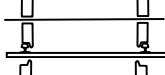
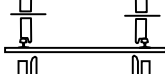
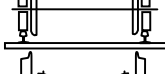
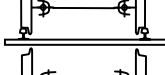
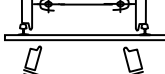

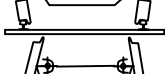
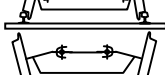
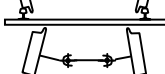
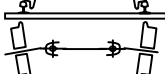
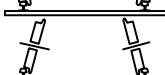
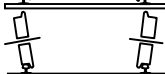
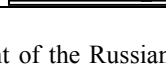
Introduction

Solving the problem of interaction in the wheel-rail system is the key task for the rail transport. Reduction of the dynamic impact of the rolling stock on the track significantly improves the safety and energy efficiency of the railway traffic. Currently, research schools approach this problem in several ways – by creating new alloys and steels, by developing recommendations for repair and maintenance of the rolling stock and track, and by creating new designs of rolling stock elements. Taking into account the advantages and disadvantages of the proposed wheel pair designs, a wheel pair of new design has been proposed. This wheel pair is designed for use on the railways with the 1,520-mm track gauge as the carrying and guiding element at the speed below 200 km/h. This assumes replacement of standard wheel pairs in the bogies of closed cars, gondola cars, platforms, and refrigerator cars with the axle load up to 23 tons with the wheel pairs of new design.

* Corresponding author. Tel.: +7 913 969 9099; fax: +7 (3812) 31-06-55.

E-mail address: shiler_alex@inbox.ru

Table 1. Classification of wheel pairs including prototypes

Design features of wheel pairs.	The scheme of the design solution.	Resistance to movement, %
1.1. Conventional with profiled tires.		Reference value 100
1.2. Conventional with cylindrical tires.		130
1.3. With free wheels and profiled tires.		75
1.4. With free wheels and cylindrical tires.		75
1.5. A wheel pair with separate drive and profiled tires.		75
1.6. With the wheel treads and flanges rotating independently of each other.		50
1.7. A wheel pair with profiled tires.		90
1.8. A wheel pair with cylindrical tires.		120
2.1. With free angled wheels and profiled tires.		75
2.2. With free angled wheels and cylindrical tires.		75
2.3. With angled wheels and profiled tires.		90
2.4. With angled wheels and conical tires.		90
2.5. A pair of angled wheels with profiled tires.		90
2.6. A pair of angled wheels with conical tires.		75
2.7. A pair of free angled wheels with separate drive and profiled tires.		75
2.8. A pair of free angled wheels with separate drive and conical tires.		75

Structurally, the new wheel pair complies with the patent of the Russian Federation "Rail transport wheel» No. 2207250 of 2003. Schematically, the design is shown in Fig. 1. The figure shows that the wheel pair of the new design consists of an axis (8), on which two flange discs (3) are tightly press-fitted, and two wheels (5), which are in resting contact with the single axis (8) by means of their own bearing assemblies (13). The wheel has a flexible tire (1) on an elastic base (11). Distortion of the tire under the radial load results in increasing area of the patch of contact with the rail, and the tire itself is able to absorb the dynamic impact of the track. Thus, the stress is reduced in the contact area, the braking force transmission is improved, and the impact on the track structure and the bolster structure of the vehicle during the movement is mitigated.[5, 6].

The flange discs are designed only for taking up the transverse guiding forces and are able to rotate independently of the wheels together with the axle in the journal bearings. The wheels are intended primarily for the transmission of radial forces and the braking torque. This technology allowed avoiding spurious slip of the contact surfaces on the

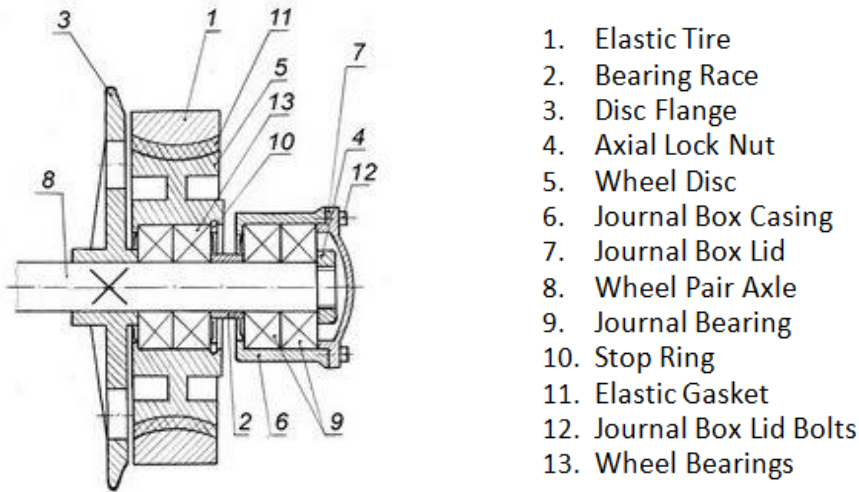


Fig. 1. Construction of new wheel pair

rail when driving with two-point contact, getting rid of the meandering movement, and reducing resistance to movement of the wheel pair, thereby improving the movement safety. Let us consider the determination of the flange disc shape.

1. Flange disc

1.1. Determination of the guiding force value

Flange discs in the new design wheel pair are segregated from the wheel and intended only for the taking up the horizontal shear forces from the track. To determine the forces exerted on the vehicle and the rail track depending on the set speed of motion on a curve, the so-called dynamic guiding of the vehicle in curve is carried out [1, 2]. At that, the greatest forces arising during the movement of the vehicle on a curve are determined, and for this purpose the following assumptions are made. The motion speed is assumed constant; the curve is assumed an ideal circular curve. All the forces exerted on the vehicle are transferred to the track plane. The friction forces at the point of contact of the wheel with the rail are constant when moving on a curve. All wheel pairs (axes) are fastened rigidly to the vehicle frame, i.e. they cannot move relative to each other either longitudinally or transversely. Traction and braking forces are absent. As an example, let us consider the motion of a bogie with wheel pairs of new design in the rail gauge in the case of loose-fitting (Fig. 4 [1, 2]).

The first wheel pair rides on the outer rail and as a result of this interaction, the guiding force Y_1 impacts on the wheel pair, which force is to be found. The movement of the vehicle on a curve can be regarded as rotation around the curve center O . Let us decompose this movement into the translational and rotational movement around a certain point Ω – the instantaneous center of rotation. This point is characterized by a minimum of forces Y_i , required to turn the bogie; therefore, it should be located at the intersection of the longitudinal axis of the vehicle and the radius perpendicular to it. When the bogie turns around the instantaneous center of rotation Ω , the forces F_i emerge in the reference points, which forces can be decomposed into the longitudinal V_i and transverse H_i components (i is the wheel pair number). The frictional forces are directed opposite to the bogie rotation. In a bogie with conventional wheel pairs, V_i and H_i are equal to the product of the sliding friction factor (which was calculated as equal to 0.25) by the value of load of the wheel on the rail P and $\sin\alpha$ (4.12) or $\cos\alpha$, accordingly. But in the bogie with wheel pairs of

new design [3], $V_i \ll H_i$, because the longitudinal reaction is represented by the forces of rolling friction, and the shear reaction – by the forces of sliding friction. Therefore, when determining the guiding force exerted by the track on the bogie with the wheel pairs of new design, we can neglect the longitudinal forces at the contact points V_i .

In figure 2 [1, 2], x_i is the distance from the instantaneous center of rotation to the i -th wheel pair; a is the distance from the instantaneous center of rotation O to the vehicle mass center C ; F_{oe} is the resultant of the centrifugal force and the component of the vehicle weight emerging at elevation of the outer rail above the inner one to balance the centrifugal force; M_{bs} is the drag torque occurring in the elements of spring suspension of the bodywork stage during rotation of the bogie with respect to the body.

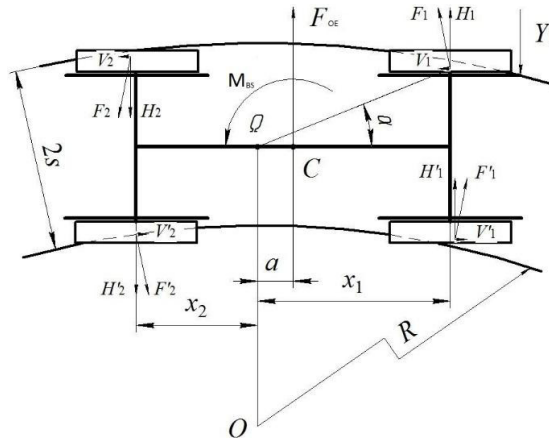


Fig. 2. Position of loose placement of the bogie in the curve

The resultant F_{oe} is defined as [2]:

$$F_{oe} = \left(\frac{P}{g}\right) \cdot \left[\frac{v^2}{R} - \frac{hg}{2s}\right], \quad (1)$$

where P is the weight of the vehicle bolster structure.

The equations of equilibrium of forces and torques for the loose placement of a bogie with wheel pairs of new design:

$$F_{oe} - Y_1 = 0 \quad (2)$$

$$M_{bs} + F_{oe}a + (H_1 + H'_1)x_1 + (H_2 + H'_2)x_2 - Y_1x_1 = 0 \quad (3)$$

These two equations have three unknowns: x_1 , v , Y_1 . In order to obtain an unambiguous solution, we must be given one unknown. If we assume that the bogie has taken chordal position, but when $Y_2 = 0$, then $x_1 = B/2$, where B is the stiff wheelbase of the bogie, i.e the distance between the outer wheel pairs. Under this condition, F_{oe} and Y_1 , and then v_1 are to be found. Further, we can find all forces Y_1 and Y_2 at $v > v_1$, as in this case F_{oe} is found using the given values of v .

To find the forces at $v < v_1$, it is necessary to consider the position of the loose placement, which takes place after placing the bogie with the heaviest skew in the gauge. At that, the displacement of the instantaneous center of rotation of the bogie $x_0 = 2\sigma_w R/B$, where $2\sigma_w$ is the total gap in the rail gauge with account of the widening. Thereafter, we can determine the new value of x_i and solve the set of equations at $Y_2 = 0$ and find Y_1 , F_{oe} , and v_2 . Further, being given $v < v_2$, we find Y_1 and Y_2 . Proceeding similarly, we can find Y_1 in the position of loose

placement of the bogie, when $Y_2 = 0$, at that the instantaneous center displacement is equal to $x_0/2$, $x_0/3$, etc. To find the guiding forces when setting the maximum skew, we need to compose the following equations:

Table 2. The value of the guiding force

Type of the wheel pair in the bogie	Speed v , km/h	Speed v , m/sec	Swaying force F^{oe} , N	Guiding force Y_2 , N	Guiding force Y_1 , N
$R=350$ m, $h=0.1$ m, $2s=1540$ mm					
Wheel pairs of new design	50.0	13.9	-3950	58382	54433
	75.0	20.8	27741	42537	70278
	86.4	24.0	46400	33207	79608
	100.0	27.8	72108	20353	92462
	118.4	32.9	112815	0	112957
	125.0	34.7	129152	8168	120983
	150.0	41.7	198872	43029	155844
Standard wheel pairs	50.0	13.9	-3950	-45537	60215
	69.2	19.2	18900	-	151200
	79.2	22.0	34309	0	167000
	100.0	27.8	71700	18810	185700
	125.0	34.7	128700	47300	214200
150.0	41.7	198400	821700	249000	
$R=600$ m, $h=0.06$ m, $2s=1520$ mm					
Wheel pairs of new design	50.0	13.9	-3024	57919	54896
	75.0	20.8	15463	48676	64139
	100.0	27.8	41343	35736	77079
	101	28.9	45778	33519	79296
	125.0	34.7	74619	19098	93717
	148.6	41.3	112815	0	112815
	150.0	41.7	115289	1237	114052
Standard wheel pairs	50.0	13.9	-3024	-37485	63734
	67.464	18.74	9113	-	140500
	93.6	26.00	34000	0	167000
	100	27.78	41330	3624	170500
	125	34.72	74570	20240	187100
	150	41.67	115300	40590	207400

$$F_{oe} + Y_2 - Y_1 = 0 \tag{4}$$

$$M_{bs} + F_{oe}a + (H_1 + H'_1)x_1 + (H_2 + H'_2)x_2 - Y_1x_1 - Y_2x_2 = 0, \tag{5}$$

where Y_2 is the guiding force of the external rail exerted on the second wheel pair. The solution of equation systems gives the values of the guiding force shown in Table 2. The bogie wheelbase was taken as 2 m, which is the maximum possible at operation of a two-axle bogie, the wheels' rolling circle diameter – 950 mm, the load – 23 tons per axle, the gauge widening on a curve to 1540 mm. After analyzing the calculated data, we can conclude that in contrast to the bogie with standard wheel pairs, the turning of a bogie with wheel pairs of new design on a curve requires less guiding force exerted by the track. To find the guiding forces at chordal placement, we need to compose the following equations:

$$F_{oe} - Y_1 - Y_2 = 0 \quad (6)$$

$$M_{bs} + F_{oe}a + (H_1 + H'_1)x_1 + (H_2 + H'_2)x_2 + Y_2x_2 - Y_1x_1 = 0 \quad (7)$$

1.2. The computational model of the flange disc

To determine the diagrams of the volume-stress state of the flange disc and optimization of the shape, we used the method of finite elements. The computational model is a disc of irregular shape with a central hole for a tight fit on the wheel pair axle and the flange following the shape of the standard wheel pair flange at the periphery of the disc.

To reduce the dimension of the problem while retaining sufficient precision of the calculations, the computational model includes only half of the flange disc severed by the vertical plane passing through the axis of the disc and the center of the contact patch. Also, in order to use a faster static equation solver that is less demanding on the hardware capabilities (the quasi-static formulation of the problem), the contact patch is a dedicated surface of the flange of small area with permanent borders throughout the entire solution of the problem. This allowed also to avoid considering the rail in the computational model and replace it with the appropriate boundary conditions.

The first version of the computational model that has already passed the shape optimization is shown in Fig. 5. shows the finite element mesh and boundary conditions for solving the problem.

It can be noted (Fig. 3 (a)) that the middle portion of the disc is tilted with respect to the vertical plane – this allows increasing the stiffness of the disc at eccentric application of force in the area of contact of the flange disc's flange with the side surface of the rail at taking up the transverse forces exerted on the wheel pair by the track. In the areas of transition of the thinner middle portion of the disc to the more massive inner portion and to the flange, fillets are made to achieve smooth distribution of stresses in these areas and to prevent their concentration.

The finite element mesh is sufficiently dense (Fig. 3 (b)); besides, the mesh control element is used for the purpose of its compaction in the areas of the fillets and the contact patch area.

The boundary conditions of the *Symmetry* type are used for the face, which is the result of clipping a half of the computational model (Fig. 3 (b)); they prohibit normal movements to this face. The boundary condition of the *Fixed* type was applied to the internal aperture, which condition prohibits movements by all the three coordinates and turning, as this is the surface, by which the flange mates with the axis (which is taken as absolutely stiff in the calculation) by tight press-fitting. The force of 50 kN was applied to the contact patch along the axis of the disc, which is half of the calculated value defined in 2.2, as in the computational model, only half of the disc takes up the load.

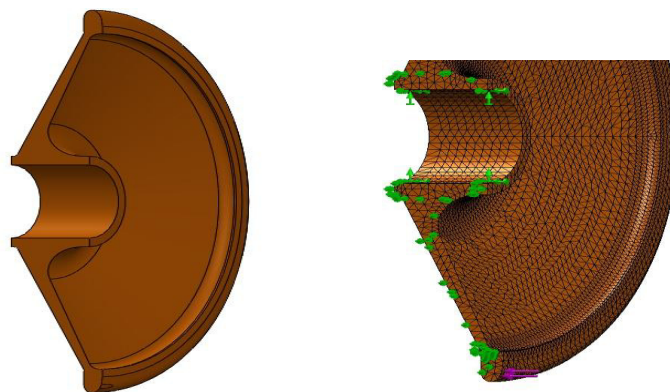


Fig. 3. (a) The computational model (version 1); (b) The finite element mesh and the boundary conditions of the model.

As a result of the calculation, we obtained diagrams of the three-dimensional state of stress (Fig. 3 (a)) and the resultant displacements (Fig. 3 (b)).

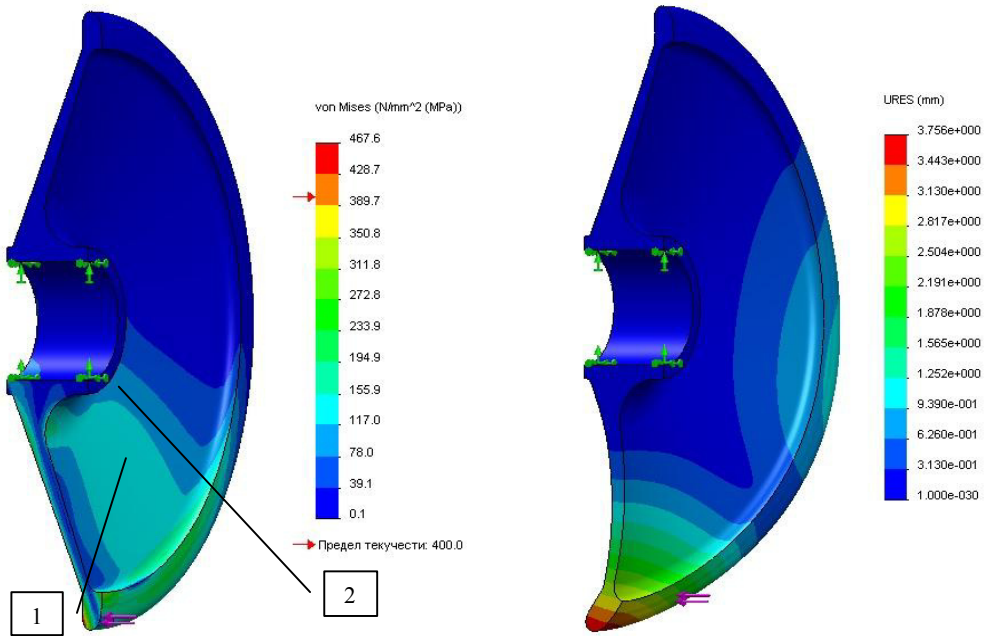


Fig. 4. (a) Wheel flange stress simulation modelling

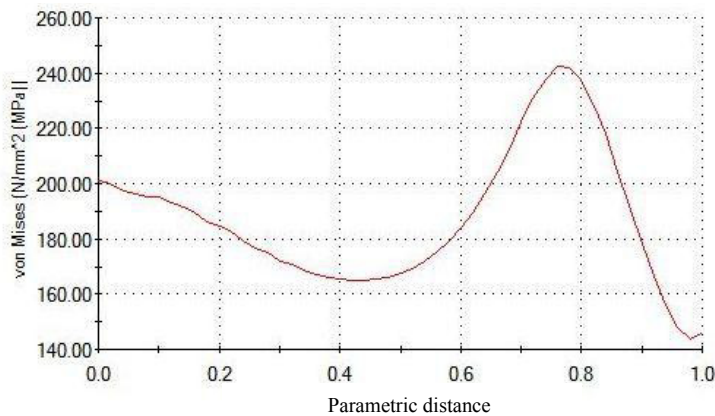


Fig. 5. The stress distribution along the edge 1.

The maximum stresses on the diagram (Fig. 4 (a)) are shown in the area of the flange on the back side from the patch of contact of the flange with the rail. It is caused by the peculiar features of imposition of boundary conditions. The material in this zone is sandwiched between the face with the imposed *Symmetry* restriction, which face does not allow normal displacements, and the rest body of the flange with similar stiffness in the plane of the disc. These stresses are overestimated and, therefore, are not taken into consideration. Checking by application of full guiding force to the complete model of the flange disc showed that the stresses in this area are lower than in the area of transition of the middle portion of the disc to the portion with the mounting hole.

To visualize the stresses, which arise in hazardous sections of the flange disc, we can derive a graph of stress distribution by the edges 1 and 2 (Fig. 4 (a)). The parametric distance is plotted on the abscissa axis, where the full length of the edge is taken as 1, and the stresses value in MPa occurring at the nodes of the finite element mesh lying on this edge is plotted on the ordinate axis. Please refer to Fig. 6 for the edge belonging to the outer surface of the middle portion of the disc (edge 1), and to Fig. 3 for the edge belonging to the fillet under the mounting hole (edge 2).

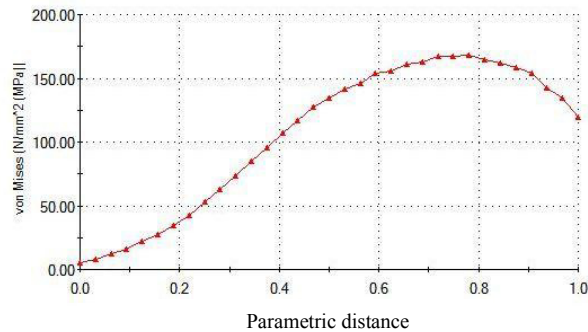


Fig. 6. The stress distribution along the edge 2.

The graphs in Fig. 5 and Fig. 6 show that the greatest stresses occur on the outer surface of the middle portion of the disc at the junction of the inner portion to the middle portion (Fig. 4 (a)), and reach 242 MPa, which is less than the allowable bending stresses equal to 291.2 MPa defined in 2.3. Stresses on the fillet at the transition of the inner portion of the disc to the middle portion on the inner side (Fig. 4 (b)) are slightly lower and do not exceed 170 MPa.

The flange is exposed to the greatest displacements (Fig. 5). At that, the axial displacement of its outer portion is equal to 3.6 mm, though for a standard all-rolled wheel, the axial displacement of the flange at the same guiding force is equal to 0.9 mm. The flange disc of such shape is more pliable to the impact of the guiding force, although the stresses do not exceed the allowable values. On the one hand, lower stiffness allows cushioning the transverse blows during movement, but, on the other hand, the combination of such withdrawal of the flange with the local widening of the gauge and rail track installation errors can result in derailing of the opposite wheel and a train wreck.

To increase the disc stiffness at the eccentric application of the force along the axis of the disc, annular ribs (Fig. 7 (a)) and radial ribs (Fig. 7 (b)) were introduced in the design. Annular ribs did not improve the stiffness to a degree sufficient to reduce substantially the movement of the flange along the axis. Radial ribs provided the required stiffness, but were too hard to manufacture. In addition, they would cause a lot of noise and aerodynamic drag at movement. It was therefore decided to abandon their use in the wheel pair of new design.

The flange displacement of an all-rolled wheel with eccentric application of force equal to 100 kN along the axis is equal to 0.9 mm. This is due to the fact that the wheel has a massive wheel tread conjugated with the flange; this massive stiff ring at the periphery of the disc distributes the guiding force over a larger area of the disc and thereby provides greater overall stiffness. To use this effect in the design of the flange disc, the wheel pair of new design was improved by introducing the thickening at the periphery of the disc above the flange (Fig. 8 (a)). The thickening is made with a smooth transition to the middle portion of the disc and the flange, thus allowing to avoid extra aerodynamic drag and noise when the rolling stock moves at a high speed.

Same as for the version 1 of the flange disc, the computational model of the version 2 includes only a half of the flange disc; the contact patch is a dedicated surface of the flange of small area with permanent borders throughout the entire solution of the problem; the rail is not considered in the calculations, and the *Static* solver is used.



Fig. 7. (a) The flange disc with annular ribs (rear view); (b) The flange disc with radical ribs (rear view).

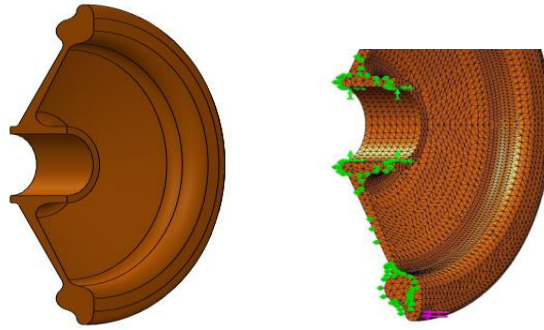


Fig. 8. Diagrams of the three-dimensional state of stress (a) and the resultant displacements (b).

As a result of the calculation, we obtained diagrams of the three-dimensional state of stress (Fig. 8 (a)) and the resultant displacements (Fig. 8 (b)). Figure 8 (b) shows the finite element mesh and boundary conditions for solving the problem. The finite element mesh is sufficiently dense (Fig. 8 (b)); the mesh control element is used for the purpose of its compaction in the areas of the fillets and the contact patch area.

The boundary conditions of the *Symmetry* type are used for the face, which is the result of clipping a half of the computational model (Fig. 8 (b)); they prohibit normal movements to this face. The boundary condition of the *Fixed* type was applied to the internal aperture, which condition prohibits movements by all the three coordinates and turning, as this is the surface, by which the flange mates with the axis (which is taken as absolutely stiff in the calculation) by tight press-fitting. The force of 50 kN was applied to the contact patch along the axis of the disc, which is half of the calculated value defined in 2.2, as in the computational model, only half of the disc takes up the load.

To visualize the stresses, which arise in hazardous sections of the flange disc, we can derive a graph of stress distribution along the edges 1 and 2 (Fig. 11 (a)). The parametric distance is plotted on the abscissa axis, where the full length of the edge is taken as 1, and the stresses value in MPa, which occurs at the nodes of the finite element mesh lying on this edge, is plotted on the ordinate axis. Please refer to Fig. 12 for the edge belonging to the outer surface of the middle portion of the disc (edge 1), and to Fig. 10 for the edge belonging to the fillet under the mounting hole (edge 2).

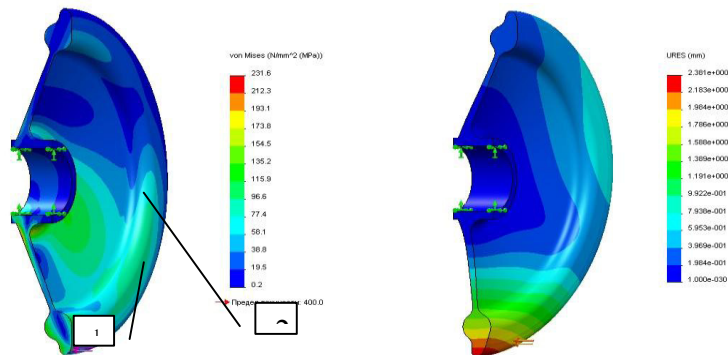


Fig. 9. (a) Diagram of the three-dimensional state of stress (the deformation scale 1:1); (b) Diagram of the resultant displacements (the deformation scale 40:1)

The location of areas with high stresses has not changed, and the value of the stresses remains at the same level compared to the flange disc of version 1, but the thickness of the middle portion of the disc has become less and the radius of transition of the middle portion to the inner one with a mounting hole has also significantly decreased.

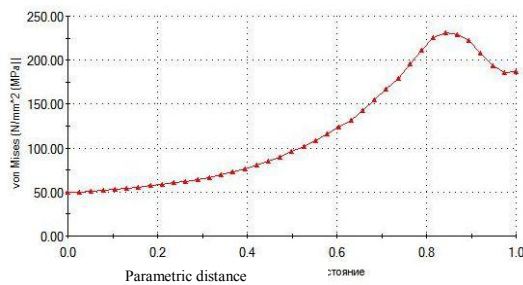


Fig. 10. The stress distribution along the edge 1

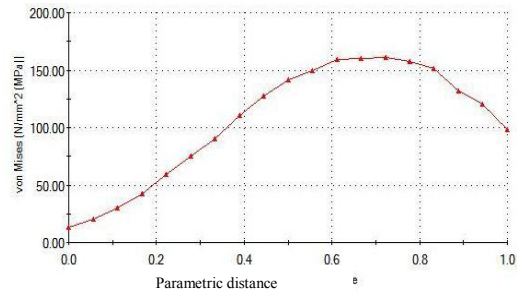


Fig. 11. The stress distribution along the edge 2

Thus, we have managed to achieve reduction of material consumption for these areas and reduce the mass of the whole disc, although the total mass of the disc of version 2 is 21.4% larger than that of version 1. Conclusions should state concisely the most important propositions of the paper as well as the author's views of the practical implications of the results. The main achievement of the introduction of the thickening at the periphery of the disc is the increased stiffness from the eccentric application of the guiding force and the reduced release of the flange to 2.3 mm (see. Fig. 11 (b)), which is 1.4 mm less than that of version 1. But further "build-up" of the thickening will result in significant increase in the weight of the wheel pair of new design, which would adversely affect the vertical dynamics of the rolling stock and significantly increase the dynamic impact on the track.

Conclusion

This study included analysis of all the proposed versions of wheel pair designs. To reduce the dynamic impact in the wheel-rail system, we proposed a brand new design of the wheel pair. A detailed study of one of the main elements of the wheel pair – the flange disc – allowed drawing the following conclusions:

- according to the calculated data, a bogie with the wheel pairs of new design requires less guiding force to be exerted by the track for turning in a curved section of the track, than a bogie with standard wheel pairs.
- the maximum stresses emerge in the flange area on the back side from the patch of contact of the flange with the rail and reach 242 MPa, which is less than the allowable bending stress equal to 291.2 MPa. The axial displacement of the outer portion of the flange is equal to 3.6 mm. The axial displacement of the flange of a standard all-rolled wheel with the same guiding force is equal to 0.9 mm.
- to increase the stiffness of the flange disc, the peripheral thickening was introduced in its design. The thickening was made with smooth transition to the middle portion of the disc and the flange. This shape is easily manufactured by rolling and reduces the flange disc weight. Release of the flange by the guiding force decreased to 1.9 mm, which is substantially less than in the case of other versions of the flange disc.

In the future, we plan to undertake a study of the elastic gasket of the wheel disc, prototype the wheel pairs, and provide the performance tests.

References

- [1] Patent No. 51563 (Russia) Wheel pair of a Rail Vehicle / Maria Anatolyevna Kolga (RU), Viktor Vasilyevich Tochilkin (RU), Anatoly Dmitriyevich Kolga (RU), Konstantin Nikolayevich Vdovin (RU). Patent published on: 27.02.2006
- [2] Patent No. 61639 (Russia) Wheel pair of Railway Rolling Stock / Grigory Ivanovich Petrov (RU), Alexander Grigoryevich Petrov (RU), Oleg Grigoryevich Petrov (RU). Patent published on: 10.03.2007
- [3] Patent No. 955989 (Russia) Wheel pair of a Car Having Independent Wheels Rotation / Oleg Valeryevich Melnichenko (RU), Yegor Vladimirovich Chuprakov (RU), Yuri Vladimirovich Gazizov (RU), Sergey Anatolyevich Gorbatok (RU), Viktor Alexandrovich Erofeev (RU). Patent published on: 10.07.2010
- [4] Patent No. 2400373 (Russia) Car Wheel pair / Evgeny Vasilyevich Slivinskiy (RU), Stepan Nikolaevich Velisevich (RU). Patent published on: 27.09.2010
- [5] Shiler, V. V.; Shiler A. V. (2012) The new design of the wheel set for the railway transport (In Russian), *journal tehnika zheleznih dorog*, ISSN: 1998-9318, vol. 4, pp 64 – 73, Moscow
- [6] Asplund, M., Palo, M., Famurewa, S., & Rantatalo, M. (2014). A study of railway wheel profile parameters used as indicators of an increased risk of wheel defects. *Proceedings of the Institution of Mechanical Engineers, Part F: Journal of Rail and Rapid Transit*, DOI: 10.1177/0954409714541953